Nanoscale

Accepted Manuscript

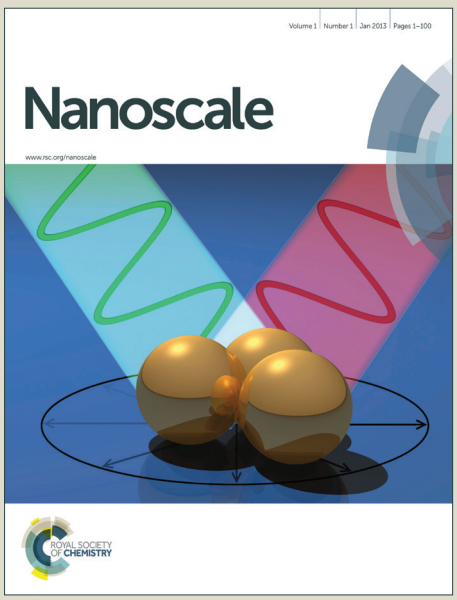

ROYAL SOCIETY OF CHEMISTRY

www.rsc.org/nanoscale

Journal Name

ARTICLE

Supramolecular helical nanofibers assembled from a pyridinium-functionalized methyl glycyrrhetate amphiphile

Received 00th January 20xx,
Accepted 00th January 20xx

DOI: 10.1039/x0xx00000x

www.rsc.org/

Yuxia Gao,[a] Jie Hao,[a] Jindan Wu,[a] Xun Zhang,[a] Jun Hu*[b] and Yong Ju*[a]

A glycyrrhetate-containing amphiphile, **MGP** (1-[2-(methyl glycyrrhetate)-2-oxoethyl]pyridinium bromide), has been synthesized, and found to assemble into supramolecular helical nanofibers in chloroform/aromatic solvents, which are primarily driven by π-π stacking, van der Waals forces, and hydrophobic interactions. During the assembly process, **MGP** stacked into *J*-aggregates resulting in the sequestration of the hydrophilic pyridinium cation within the interior with the concomitant projection of its hydrophobic skeleton on the outside surface. Ultimately, this protrusion generated a staggered angle due to the steric hindrance between stacked molecules. This staggered angle further lead to the molecular misalignments and the formation of helical fibrils, which could twist with each other to fabricate larger helical fibers. Consequently, a gel was formed by intertwining these naonfibers into three-dimensional networks. Using this strategy, we find that other triterpenoid-tailored pyridinium amphiphiles are also potential scaffolds for supramolecular helical structures. This work provides a facile approach for the fabrication of supramolecular macroscopic chiral nanostructures that originate from natural products.

Introduction

Triterpenoids, one class of naturally occurring compounds with 30 carbon atoms, can be biosynthesized from squalenes as the common precursor, and are found in many plants in the form of free acids or aglycones.[1] They have attracted immense attention due to their relative low-toxicity and fascinating anti-virus, anti-tumor, and anti-inflammatory properties.[2] Recently, the focus has begun to shift to their supramolecular behaviors owing to their rigid skeleton, multiple functional groups, and unique stacking manners.[3] The skeletons of triterpenoids are lined with readily accessible hydroxyl and carboxyl groups, which allows for the facile introduction of functional units to promote non-covalent interactions and engender supramolecular assemblies. In this regard, Bag[3,4] and our group[5] have developed a series of triterpenoid-based supramolecular assemblies over the past ten years. Notably, the abundance of chiral centers upon the skeleton makes triterpenoids ideal candidates for the fabrication of supramolecular chiral structures *via* self-assembly. To date, very little research has been devoted to triterpenoid-based supramolecular macroscopic chiral nanostructures.[4,6] Bag and co-workers have observed some partial helical ribbons when they studied the relationship between the molecular components and gelation abilities of betulinic acid (**BA**)/oleanolic acid (**OA**) (two kinds of triterpenoids), but no in-depth investigation of the mechanism was explored.[4] Recently, Mezzenga and co-workers found that the right-handed fibrillar networks of natural glycyrrhizic acid could be utilized as scaffolds for hybrid nanomaterials in heterogeneous catalysis as we prepared our work.[6] This result verifies that the fabrication of supramolecular macroscopic chiral structures originated from triterpenoids and may open new scenarios in advanced materials. Thus, it is necessary and beneficial to explore a strategy to realize the chirality transfer from molecules to nano/macro-scale using triterpenoids as building blocks.

One attractive approach is to learn from amphiphiles. Containing hydrophilic and hydrophobic units, amphiphiles have proven to be an important type of building blocks in well-defined supramolecular structures,[7] primarily driven by the combination of various non-covalent interactions including π-π stacking, van der Waals forces, hydrogen bonding, electrostatic attractions, charge-transfer interactions, and hydrophobic interactions.[8] Specifically, amphiphiles containing biological skeletons attain more interests because of their inherent chiral centers, multiple reactive sites, relative low-toxicity, and biocompatibility. For example, Xu and co-workers have built up a hydrogel on the surface of cancer cells by the enzyme-induced assembly of a naphthalene-D-peptide amphiphile.[9] This hydrogel can block the cellular mass exchange, which induced the apoptosis in cancer cells. In our previous work, different organogels and hydrogels were

[a] *Key Laboratory of Bioorganic Phosphorus Chemistry & Chemical Biology, Ministry of Education, Department of Chemistry, Tsinghua University, Beijing 100084, China. E-mail: juyong@tsinghua.edu.cn.*
[b] *State Key Lab of Polymer Physics and Chemistry, Changchun Institute of Applied Chemistry, Chinese Academy of Sciences, Changchun 130022, China. E-mail: jhu@ciac.ac.cn.*

† Electronic Supplementary Information (ESI) available: Synthetic routes and structure characterizations of **MGP**, **MGBP**, **C4-MGP**, and **C4-MOP**; Additional TEM images and spectroscopic data on self-assembly of **MGP** in various solvents. See DOI: 10.1039/x0xx00000x

constructed either from glycyrrhetinic acid (**GA**, another kind of triterpenoids) or **OA** derivatives, however, no supramolecular chiral structures were observed.[5] It is assumed that the steric repulsion between skeletons and an insufficient amount of driving forces hindered the molecular chirality transfer to nano/macro-scale. Inspired by the aforementioned work, we hypothesized that a strong non-covalent interaction combined with a relatively compact molecular volume will coordinate with triterpenoid-scaffolds to generate supramolecular chiral structures.

Of all the non-covalent interactions, π-π stacking is normally stronger than van der Waals forces, and the relatively compact volumes of aromatic rings can reduce the steric repulsion. In addition, the overlap between aromatic rings possesses a predictable self-assembly behavior by adopting a plane-to-plane or an edge-to-plane orientation.[10] Herein, we designed and synthesized a π-chromophore-containing glycyrrhetinic acid amphiphile 1-[2-(methyl glycyrrhetate)-2-oxoethyl]pyridinium bromide, **MGP** (Fig. 1, synthetic details see ESI), where **GA** is connected to an aromatic pyridinium cation by a short alkyl chain. Within this molecule, the pyridinium cation is not only used to enhance the molecular hydrophilicity, but is also the origin of π-π stacking;[11] whereas the short alkyl chain restricts the molecular rotation of the assembly in comparison to other long flexible chains. Our results demonstrated that **MGP** self-assembled into well-ordered supramolecular helical nanofibers in a mixture of chloroform and aromatic solvents. This behavior is driven by the combination of π-π stacking, van der Waals forces, and hydrophobic interactions. Moreover, these helical nanofibers can further entangle with each other to generate the transparent gels as shown in Fig. 1. This work illustrates a facile methodology for creating supramolecular chiral nanostructures that originate from natural products.

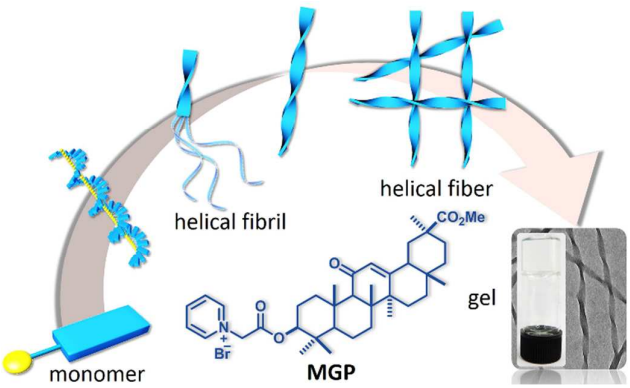

Fig. 1 Schematic representation of the fabrication of supramolecular helical nanofibers from amphiphilic **MGP**.

Results and discussion

Preparation of the supramolecular gel

As a general protocol, **MGP** was dissolved in chloroform to form a clear solution followed by the gradual addition of the aromatic solvents. After the addition, the mixture was incubated at room temperature without heating or ultrasound. It was found that **MGP** could form gel under any of the tested mixed solvents of chloroform and aromatic solvent (toluene, *o*/*m*/*p*-xylene, mesitylene, chlorobenzene, bromobenzene, and *o*-dichlorobenzene). The optimal volume proportions between chloroform and aromatic solvents are summarized in Table S1, as well as their minimum gelation concentrations (MGC).

Study of the morphology and the chirality

Transmission electron microscopy (TEM) was employed to investigate the gel morphologies. Entangled helical nanofibers could be observed clearly, where the pitch was around 120 nm, with the length at several micrometers, and the width varying from 28 to 40 nm (Fig. 2 and Fig. S1). It should be noted that the helices handedness in each solvent system is different as listed in Table S2. Both left- (*M*) and right-handed (*P*) helices exist in *o/m/p*-xylene, chlorobenzene, and bromobenzene systems, respectively (Fig. 2a, b and Fig. S1a-c). Conversely, either *M* or *P* helices are found in toluene, mesitylene, and *o*-dichlorobenzene systems (Fig. S1d and Fig. 2c, d), respectively. Spectra from circular-dichroism (CD) afford more direct insights into the assembly handedness since the Cotton effect signs can be used as a probe for the chirality and stereochemical assignments.[12] As shown in Fig. S2, the similar intensive negative Cotton effect at the lower wavelength and the weak positive Cotton effect at the higher wavelength appear in *o/m/p*-xylene, chlorobenzene, and bromobenzene systems; while two positive Cotton effects are observed in toluene or mesitylene, and only two negative Cotton effects are found in *o*-dichlorobenzene. These results reiterate the differences between the helices in each solvent system, which are in exact agreement with our TEM analysis. It is well-known that the handedness of supramolecular helices depends not only on the molecular chirality, but also the orientation of molecular tilts which can be affected by molecular geometries, solvents, ultrasound, ions, *etc.*[13] When the tilt direction changes, the curvature, the width, and the pitch of aggregates will change accordingly. Therefore, it is proposed that the different handedness of helical nanofibers from enantiomerically pure **MGP** is due to the different molecular tilt orientation induced by solvents.

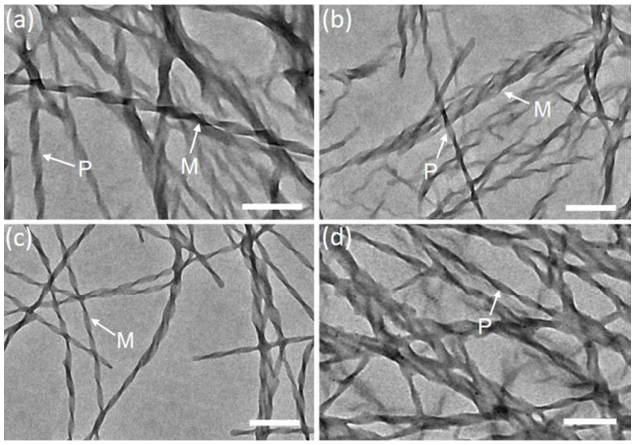

Fig. 2 TEM images of **MGP** assemblies in mixed solvents of chloroform and (a) *o*-xylene, (b) *m*-xylene, (c) mesitylene, (d) *o*-dichlorobenzene (chloroform/ aromatic solvent = 1: 2, v/v, 12 mM). Scale bar is 200 nm.

To better understand the assembly process, morphologies of **MGP** were evaluated by TEM images as functions of volume ratios and concentrations. As shown in Fig. 3a, wavy fibrils having the potential spiral trend with a diameter around 12 nm appear in chloroform solution. With the addition of *o*-xylene into chloroform solution, these fibrils progress into robust fibers accompanied by the diameter increasing and numerous tiny fibers intertwining (Fig. 3b). Upon the continuous addition, the irregular fibers curve along a certain direction, and consequently form the well-ordered helical fibers when the ratio of *o*-xylene reaches 67 % (Fig. 3c, d). It is believed that with the increase of poor solvents **MGP** orients in a way that expose the hydrophobic **GA** skeleton to the solvent, whereas the hydrophilic pyridinium within the interior is embedded on account of the amphiphilic nature of **MGP**. Furthermore, TEM images of **MGP** in chloroform/*o*-xylene (1:2, v/v) clearly reveal the transformation pathway from threadlike twists to helical fibrils, helical fibers, and gels, with the increase in concentration as shown in Fig. S3.

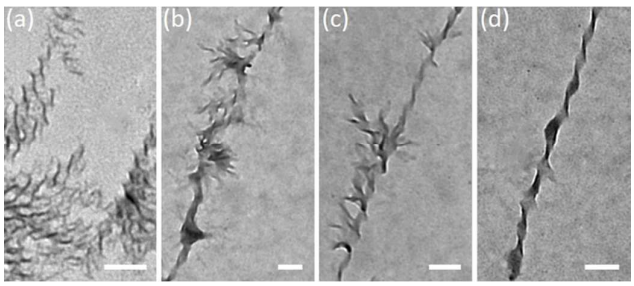

Fig. 3 TEM images of **MGP** assemblies at different volume ratios of chloroform/*o*-xylene (7 mM): (a) 2:0, (b) 2:1, (c) 2:2, and (d) 2:4. Scale bars are 200 nm for (a), (b), (c), and 100 nm for (d).

Investigation of the driving force

To probe the driving forces outside of the hydrophobic interactions, ^{1}H NMR, UV-Vis, and FT-IR experiments were performed. As shown in Fig. 4a, with the increase in concentration of **MGP** in deuterated chloroform/*o*-xylene, the proton signals of pyridinium (H_1, H_2, H_3) move downfield, revealing the π-π stacking between pyridinium moieties.[14] Additional evidences for π-π stacking come from UV-Vis spectra. A significant red-shift from 250 to 295 nm is observed with the increase in *o*-xylene content as shown in Fig. 4b. This is indicative of the formation of *J*-type aggregates through π-π stacking between pyridinium rings.[15] Similar red-shift features in absorption spectra of **MGP** are attained in the other mixed solvents when the concentration increases from 5.0×10^{-5} to 1.5×10^{-3} M (Fig. S4), and these values are listed in Table S3. Moreover, FT-IR spectra show that the saturated C-H stretching vibrations of the methyl groups located on **GA** skeleton move from 2952, 2878 cm^{-1} to 2942, 2875 cm^{-1} (Fig. 4c), respectively, upon the formation of helical fibers. It is known that the stretching vibrations of alkyl groups can be used as a sensitive indicator for the order of alkyl chains because the increase in frequencies and band widths is closely related to the increasing numbers of gauche defects and disorder.[16] Thus, the decrease in wavenumbers from **MGP** in chloroform to helices suggests an increase in van der Waals forces between the neighboring **GA** skeletons. Given the above, it is believed that π-π stacking, van der Waals forces, and hydrophobic interactions are the major driving forces for the well-defined helical structures.

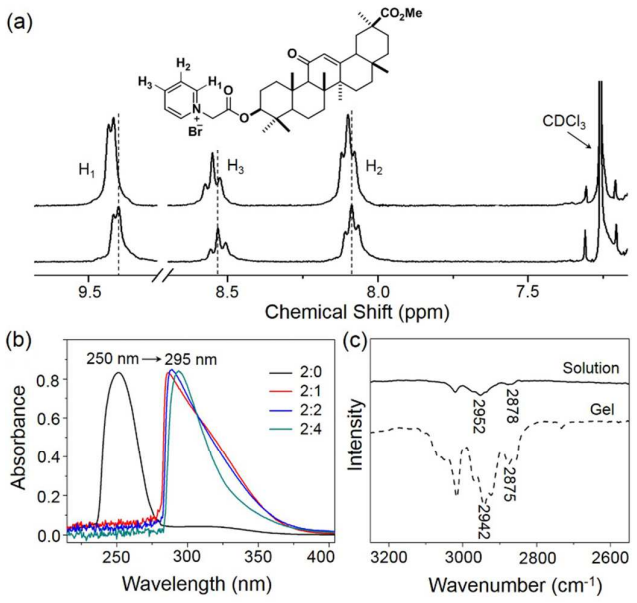

Fig. 4 (a) ^{1}H NMR spectra of **MGP** in mixed solvents of deuterated chloroform (500 μL) and *o*-xylene (1.7 μL) under different concentrations (bottom:14 mM, top: 28 mM); (b) UV-Vis spectra of **MGP** in different volume ratios of chloroform/*o*-xylene (5.0×10^{-4} M); (c) FT-IR spectra of **MGP** in chloroform solution (12 mM) and helices (chloroform/*o*-xylene = 1:2, v/v, 12 mM).

Fabrication of the packing pattern

In order to determine the packing patterns of supramolecular helical fibers, theoretical computation, X-ray diffraction (XRD), and selected area electron diffraction (SAED) experiments were carried out. Theoretical computation is a useful tool in optimizing the geometry and simulating the molecular

structure in supramolecular systems,[17] therefore, AM1 method was chosen to optimize the structure of **MGP** by Gaussian 09. As shown in Fig. 5a, the optimized horizontal length of **MGP** is 1.36 nm, and vertical distances are 0.54 and 0.57 nm, respectively, marking the pyridinium ring as the datum plane. Meanwhile, four reflection peaks corresponding to *d*-spacing of 4.30, 1.38, 0.61, 0.37 nm in XRD (Fig. 5b) and 0.61 nm in SAED (Fig. 5c) are observed, which verify the lamellar structures in the helices.

By comparing the results from our theoretical computation, XRD, and SAED, the *d*-spacing of 1.38 nm corresponds closely to the theoretical molecular horizontal length (1.36 nm), while 0.37 nm is the typical π-π stacking distance on account of the formation of *J*-type aggregates between adjacent pyridiniums[18] (Fig. 5d). Additionally, *d*-spacing of 4.30 nm is assigned to the helical pitch (Fig. 5e). Given that π-π stacking distance is 0.37 nm, it is found that nearly 12 (4.30 nm/0.37 nm) **MGP** molecules assemble into a pitch at the molecular level. Because the vertical distance of **MGP** (0.54 and 0.57 nm) is larger than π-π stacking distance (0.37 nm) between two molecules, such steric hindrance produces a staggered angle around 30° (360°/12) to fit into the space, which further leads to the molecular misalignments (Fig. 5f). Hence, the outer distance between **GA** skeletons, calculated by Gaussian 09, is precisely consistent with the *d*-spacing of 0.61 nm as shown under XRD and SAED analyses (Fig. 5f).

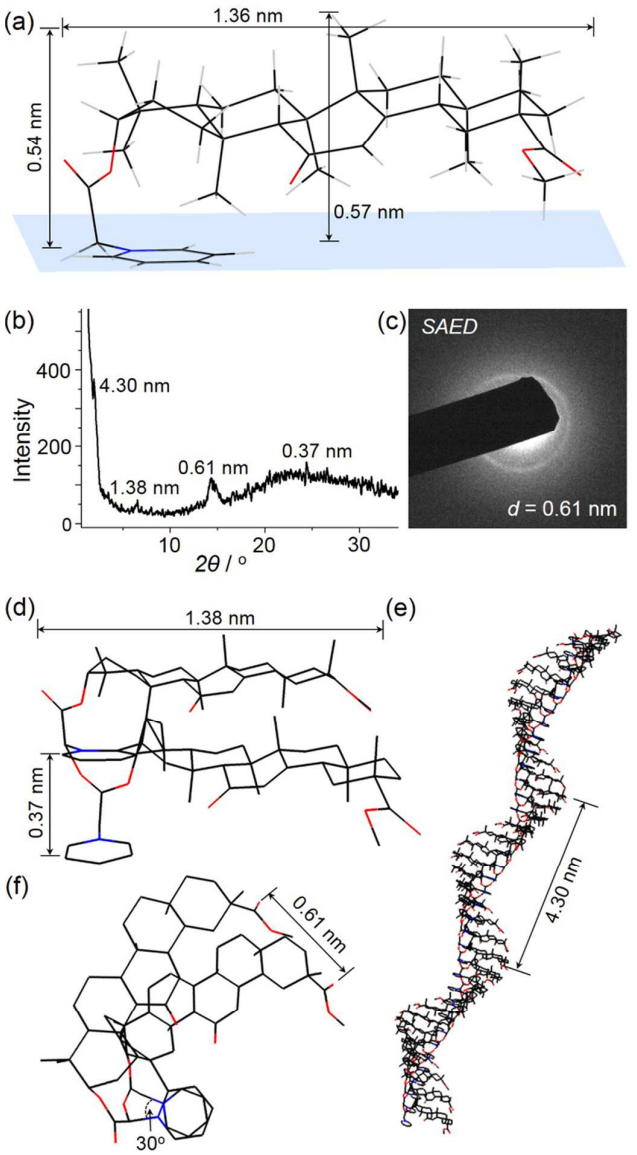

Fig. 5 (a) Theoretical optimized structure of **MGP** using Gaussian 09 AM1 method; (b) XRD and (c) SAED patterns of helices assembled from **MGP** (chloroform/*o*-xylene = 1:2, v/v, 12 mM); (d-f) Possible simulated packing modes of helices assembled from **MGP** from different views. Carbon atoms, hydrogen atoms, oxygen atoms, and nitrogen atoms are presented in black, light gray, red, and blue, respectively. Hydrogens are hided in d-f), and bromines are neglected in all modes.

Based on all the above results, it is apparent that **MGP** molecules assembled into *J*-aggregates by sequestering the hydrophilic pyridinium within the interior and projecting the hydrophobic **GA** skeleton on the outside surface. This phenomenon is primarily promoted by the combination of π-π stacking, van der Waals forces, and hydrophobic interactions. The steric hindrance during π-π stacking generated a staggered angle, thus leading to the molecular misalignments in either left-handed or right-handed manners, which were heavily influenced by molecular chirality and solvent effects. This basic unit formed by the misalignments at the initial stage (proposed in Fig. 5d-f) would stack orderly to form large helical fibrils.[19]

Consequently, the fibrils twisted with each other to construct larger helical fibers, which further intertwined into three dimensional networks to form gels as shown in Fig. 1. During this hierarchical self-assembly process, the molecular chirality of **MGP** was magnified and translated from molecular scale to nano/macro-scale,[19,20] as the macroscopic helical nanofibers we observed in TEM images.

Self-assembly of other triterpenoid-tailored pyridinium amphiphiles

Taken together, supramolecular helical nanofibers were successfully achieved by modifying a hydrophilic pyridinium group on the hydrophobic methyl glycyrrhetate skeleton, driven by π-π stacking, van der Waals forces, and hydrophobic interactions. To better verify the universality of this bottom-up strategy in fabricating chiral structures, we have synthesized other three triterpenoid-tailored pyridinium amphiphiles, 1-[2-(methyl glycyrrhetate)-2-oxoethyl]-[4, 4′]bipyridinium bromide (**MGBP**), 1-[4-(methyl glycyrrhetate)-4-oxobutyl]pyridinium bromide (**C4-MGP**), and 1-[4-(methyl oleanolate)-4-oxobutyl] pyridinium bromide (**C4-MOP**) (Fig. 6, synthetic details see ESI), where the hydrophilic group, linker, and hydrophobic triterpenoid skeleton were switched, respectively.

By investigating the self-assembly behaviors of **MGBP**, **C4-MGP**, and **C4-MOP** in mixed solvents, different helical structures were observed. As shown in Fig. 6a, right-handed helices with the width of 33 nm and the pitch around 25 nm are formed by **MGBP** in the mixed solvents of chloroform/*o*-xylene. When the linker is elongated, **C4-MGP** could assemble into well-defined left-handed helical nanofibers in chloroform/toluene with 48 and 95 nm in width and pitch, respectively (Fig. 6b); whereas **C4-MOP** can form left-handed helical ribbons in methanol/water with a diameter at 0.4 μm, and the helical pitch ranges from 0.9 to 2.1 μm (Fig. 6c). All these helical structures confirm that triterpenoid-tailored pyridinium amphiphiles are potential scaffolds for the fabrication of supramolecular helical structures. Moreover, the different morphologies reveal the effect of structure-function relationship on the self-assembly behaviors of these amphiphiles.

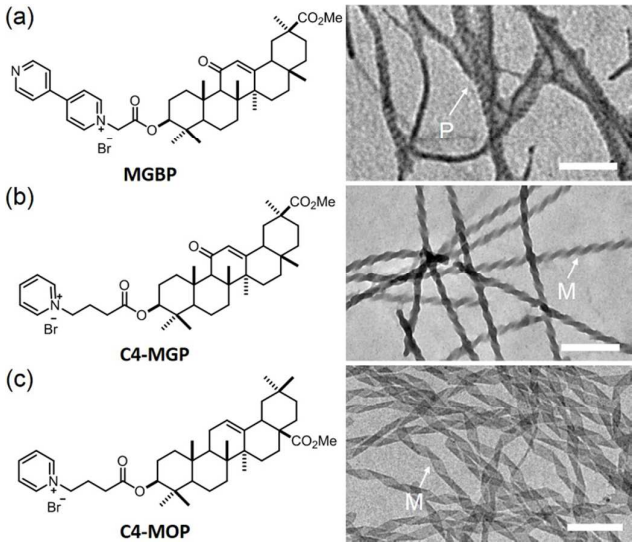

Fig. 6 Molecular structures of other triterpenoid-tailored pyridinium amphiphiles (left) and their corresponding TEM images (right) in different solvents. (a) **MGBP** (chloroform/*o*-xylene = 1:4, v/v, 13 mM); (b) **C4-MGP** (chloroform/toluene = 5:8, v/v, 11 mM); (c) **C4-MOP** (methanol/water = 1:2, v/v, 7 mM). Scale bars are 200 nm for (a), 300 nm for (b), and 2 μm for (c).

Conclusions

In summary, a pyridinium-functionalized methyl glycyrrhetate amphiphile **MGP** was synthesized, and its assembly behavior was investigated. It was found that **MGP** formed supramolecular gels in chloroform/aromatic solvents, and their self-assembly process from single molecule to fibrils, helical fibers, and gels was evaluated by TEM imaging. Spectra from ^{1}H NMR, UV-Vis, and FT-IR measurements revealed that π-π stacking, van der Waals forces, and hydrophobic interactions were the primary driving forces for the fabrication of supramolecular helical nanofibers. In conjunction with theoretical computation, XRD, and SAED results, the packing patterns were established, which revealed the roles of triterpenoids and pyridinium cations in the assembly process. Using this bottom-up strategy, we found other triterpenoid-tailored pyridinium amphiphiles were also potential assembly scaffolds for supramolecular helical structures. These results provide a facile approach in fabrication of supramolecular macroscopic chiral nanostructures, and open new scenarios on the design of advanced materials using natural precursors and affordable building blocks.

Experimental

Materials

The starting materials glycyrrhetinic acid (**GA**), oleanolic acid (**OA**), methyl iodide, bromoacetyl bromide, 4-bromobutyric acid, *N*,*N*'-dicyclohexylcarbodiimide (DCC), 4-dimethylaminopyridine (DMAP), pyridine, 4,4'-bipyridine, and other reagents were local commercial products and used as

received. All organic solvents were dried and distilled before used.

General methods

^{1}H and ^{13}C nuclear magnetic resonance (NMR) spectra were recorded on a JOEL JNM-ECA 300/400 apparatus; Electrospray ionization mass spectrometry (ESI-MS) was performed on Bruker ESQUIRE-LC spectrometer; High-resolution mass spectrometry (HRMS) was acquired using a quadrupole time-of-flight (Q-ToF) instrument; Transmission electron microscopy (TEM) images were obtained on Hitachi H-7650B electron microscope operating at the accelerating voltage of 80 kV; The samples were prepared by drop-casting the sol on the carbon coated copper grid, and then dried in air; Circular dichroism (CD) spectra were recorded on a Pistar π-180 instrument (Applied Photophysics Ltd) with a 150 w xenon lamp as the light source; UV-Vis spectra were attained on TU-1901, and FT-IR spectra were measured on a Perkin Elmer spectrum 100 FT-IR spectrometer in situ; X-ray diffraction (XRD) analysis was achieved using a Rigaku D/max 2500v X-ray diffractometer with CuKα radiation (λ = 1.5406 Å), operating at 45 kV and 100 mA; Selected area electron diffraction (SAED) was performed on JEM-2010, in which the sample preparation method was similar to that of TEM; Theoretical calculation was realized by AM1 method using Gaussian 09.

Synthesis of MGP

Intermediates **GA-CO_2Me** and **Br-GA-CO_2Me** were prepared according to our previous work (Scheme S1).[21] **Br-GA-CO_2Me** (546 mg, 0.90 mmol) was dissolved in 25 mL pyridine, and then stirred at room temperature for 10 h. After evaporating the solvent under reduced pressure, the crude product was purified by chromatography (CH_2Cl_2/CH_3OH = 20:1 to 10:1, v/v) to give **MGP** as a white solid (567 mg, 92 %). ESI-MS (+): m/z 604.5; HRMS (ESI): m/z calcd. for $C_{38}H_{54}O_5N$: 604.4002, found 604.4007; ^{1}H NMR (400 MHz, DMSO-d_6, ppm): δ = 9.13 (d, 2 × 1H, *J* = 5.96 Hz, pyridine-H), 8.72 (t, 1H, *J* = 7.76 Hz, pyridine-H), 8.26 (t, 2 × 1H, *J* = 6.88 Hz, pyridine-H), 5.75(dd, 2H, J_1 = 36.64 Hz, J_2 = 16.96 Hz, CH_2CO_2), 5.43 (s, 1H, 12-CH=C-), 4.55 (m, 1H, 3-CH-O-), 3.63 (s, 3H, OCH_3), 1.36, 1.10, 1.05, 1.03, 0.87, 0.74, 0.71 (s, 7 × 3H, 7 × CH_3); ^{13}C NMR (100 MHz, $CDCl_3$, ppm): δ = 199.96 (O=C-CH=C-), 176.96 (O=C-OCH_3), 169.58 (3-O-C=O), 165.50 (CH=C-), 146.81, 146.49, 128.15 (5C, pyridine-C), 128.42 (CH=C-), 83.74 (3-CH-O), 61.59, 61.43, 54.90, 53.55, 51.82, 48.41, 45.41, 44.08, 43.27, 41.11, 38.66, 38.26, 37.80, 36.90, 32.62, 31.87, 31.15, 28.58, 28.46, 28.36, 26.48, 23.62, 23.49, 18.71, 17.36, 16.79, 16.46.

Synthesis of MGBP

The preparation of **MGBP** was outlined in Scheme S2. **Br-GA-CO_2Me** (944 mg, 1.56 mmol) and 4,4'-bipyridine (111 mg, 0.71 mmol) were dissolved in 25 mL dry CH_2Cl_2, and then the mixture was stirred at room temperature for 24 h. After removing the solvent under reduced pressure, a brown crude was obtained, which was further purified by silica gel column chromatography (CH_2Cl_2/CH_3OH = 30:1 to 5:1, v/v) to afford **MGBP** as a light yellow solid (407 mg, 75 %). ESI-MS (+): m/z 681.6; HRMS (ESI): m/z calcd. for $C_{43}H_{57}O_5N_2$: 681.4267, found 681.4265; ^{1}H NMR (400 MHz, DMSO-d_6, ppm): δ = 9.26 (d, 2 × 1H, *J* = 6.88 Hz, bipyridine-H), 8.90 (d, 2 × 1H, *J* = 5.92 Hz, bipyridine-H), 8.75 (d, 2 × 1H, *J* = 6.84 Hz, bipyridine-H), 8.07 (d, 2 × 1H, *J* = 5.96 Hz, bipyridine-H), 5.76 (dd, 2H, J_1 = 33.48 Hz, J_2 = 16.52 Hz, CH_2-CO_2), 5.43 (s, H, 12-CH=C-), 4.60 (m, 1H, 3-CH-O-), 3.63 (s, 3H, OCH_3), 1.36, 1.10, 1.06, 1.04, 0.90, 0.75 (s, 7 × 3H, 7 × CH_3); ^{13}C NMR (75 MHz, CD_3OD, ppm): δ = 200.88 (O=C-CH=C-), 177.27 (O=C-OCH_3), 171.45 (3-O-C=O), 165.61 (CH=C-), 154.80, 150.57, 146.80, 142.08, 125.54, 122.32 (8C, bipyridine-C), 127.57 (CH=C-), 84.41 (3-CH-O), 61.53, 54.67, 51.02, 45.37, 43.97, 43.32, 41.01, 38.28, 37.92, 37.65, 36.83, 32.27, 31.63, 30.65, 27.83, 27.25, 27.19, 26.24, 25.99, 23.07, 22.53, 17.94, 17.08, 15.78, 15.63.

Synthesis of C4-MGP

The synthetic procedure for **C4-MGP** was shown in Scheme S3. After the addition of 4-bromobutyric acid (414 mg, 2.48 mmol) into a dry CH_2Cl_2 (25mL) solution of **GA-CO_2Me** (1 g, 2.06 mmol), DCC (516 mg, 2.48 mmol), and DMAP (126 mg, 1.03 mmol), the solution was stirred at room temperature for 20 h. After that, the mixture was filtered, and the filtrate was washed by water (30 mL × 2), saturated sodium bicarbonate (30 mL × 2), dried by anhydrous sodium sulfate, and evaporated to give the crude, which was further purified by silica column chromatography (Hexane/EtOAc = 25:1, v/v) to afford the intermediate **Br-C4-GA-CO_2Me** as a white solid (704 mg, 54 %). ESI-MS (+): m/z 657.5 $[M+Na]^+$; HRMS (ESI): m/z calcd. for $C_{33}H_{55}BrO_4$: 635.3135, found 635.3135; ^{1}H NMR (400 MHz, $CDCl_3$, ppm): δ = 5.65 (s, 1H, 12-CH=C), 4.51 (m, 1H, 3-CH-O-), 3.67 (s, 3H, OCH_3), 3.45 (t, 2H, *J* = 6.40 Hz, Br-CH_2), 2.49 (t, 2H, *J* = 5.48 Hz, O=C-CH_2), 2.16 (m, 2H, Br-CH_2CH_2), 1.35, 1.14, 1.13, 1.11, 0.87, 0.86, 0.78 (s, 7 × 3H, 7 × CH_3); ^{13}C NMR (100 MHz, $CDCl_3$, ppm): δ = 200.13 (O=C-CH=C-), 177.00 (O=C-OCH_3), 172.35 (3-O-C=O), 169.36 (CH=C-), 128.56 (CH=C-), 80.95 (3-CH-O), 61.77, 55.07, 51.87, 48.47, 45.46, 44.11, 43.26, 41.12, 38.81, 38.16, 37.81, 36.99, 33.01, 32.87, 32.74, 31.90, 31.20, 28.60, 28.40, 28.19, 27.97, 26.54, 26.47, 23.67, 23.43, 18.74, 17.44, 16.84, 16.49.

The synthetic procedure for **C4-MGP** was similar to that of **MGP**. **C4-MGP,** a white solid, yield 64 %. ESI-MS (+): m/z 632.6; HRMS (ESI): m/z calcd. for $C_{40}H_{58}NO_5$: 632.4315, found 632.4320; ^{1}H NMR (400 MHz, DMSO-d_6, ppm): δ = 9.09 (d, 2 × 1H, *J* = 5.48 Hz, Pyridine-H), 8.61 (t, 1H, *J* = 7.80 Hz, pyridine-H), 8.17 (t, 2 × 1H, *J* = 6.40 Hz, pyridine-H), 5.43 (s, 1H, 12-CH=C), 4.63 (t, 2H, *J* = 7.32 Hz, NCH_2), 4.42 (m, 1H, 3-CH-O-), 3.63 (s, 3H, OCH_3), 2.43 (t, 2H, *J* = 7.30 Hz, O=C-CH_2), 2.21 (m, 2H, NCH_2CH_2), 1.36, 1.10, 1.06, 1.03, 0.82, 0.75 (s, 7 × 3H, 7 × CH_3); ^{13}C NMR (100 MHz, $CDCl_3$/CD_3OD = 5:1, v/v, ppm): δ = 200.72 (O=C-CH=C-), 177.36 (O=C-OCH_3), 172.31 (3-O-C=O), 170.43 (CH=C-), 145.59, 144.88, 128.60 (5C, pyridine-C), 128.18 (CH=C-), 81.82 (3-CH-O), 61.69, 60.96, 54.97, 51.83, 45.46, 44.09, 43.28, 41.02, 38.67, 38.03, 37.69, 36.91, 32.58, 31.81, 31.03, 30.35, 28.47, 28.22, 28.06, 26.80, 26.41, 26.30, 23.50, 23.28, 18.59, 17.29, 16.61, 16.33.

Synthesis of C4-MOP

The synthetic route of **C4-MOP** was shown in Scheme S4, which was similar to that of **C4-MGP**. The intermediate **OA-CO_2Me**, a white solid, yield 97 %. ESI-MS (+): m/z 493.5 $[M+Na]^+$; HRMS (ESI): m/z calcd. for $C_{31}H_{50}O_3$: 493.3652 $[M+Na]^+$, found 493.3648; ^{1}H NMR (300 MHz, $CDCl_3$, ppm): δ = 5.27 (t, 1H, *J* = 3.78 Hz, 12-CH=C), 3.64 (s, 3H, OCH_3), 3.22 (m, 1H, 3-CH-O-), 1.12, 0.96, 0.91, 0.90, 0.89, 0.77, 0.71 (s, 7 × 3H, 7 × CH_3); ^{13}C NMR (75 MHz, $CDCl_3$, ppm): 178.39 (O=C-OCH_3), 143.86 (CH=C-), 122.45 (CH=C-), 79.08 (3-CH-O), 55.31, 51.62, 47.71, 46.80, 45.96, 41.73, 41.37, 39.36, 38.84, 38.53, 37.12, 33.95, 33.20, 32.75, 32.47, 30.78, 28.19, 27.79, 27.28, 26.03, 23.73, 23.49, 23.16, 18.42, 16.92, 15.67, 15.39.

The intermediate **Br-C4-OA-CO_2Me**, a white powder, yield 58 %. ESI-MS (+): m/z 643.6 $[M+Na]^+$; HRMS (ESI): m/z calcd. for $C_{35}H_{55}BrO_4$: 643.3162 $[M+Na]^+$, found 643.3163; ^{1}H NMR (400 MHz, $CDCl_3$, ppm): δ = 5.27 (t, 1H, *J* = 3.68 Hz, 12-CH=C), 4.50 (m, 1H, 3-CH-O-), 3.61 (s, 3H, OCH_3), 3.45 (t, 2H, *J* = 6.40 Hz, Br-CH_2), 2.48 (t, 2H, *J* = 5.92 Hz, O=C-CH_2), 2.17 (m, 2H, Br-CH_2CH_2), 1.12, 0.92, 0.91, 0.89, 0.85, 0.71 (s, 7 × 3H, 7 × CH_3); ^{13}C NMR (100 MHz, $CDCl_3$, ppm): 178.36 (O=C-OCH_3), 172.36 (3-O-C=O), 143.88 (CH=C-), 122.29 (CH=C-), 81.26 (3-CH-O), 55.34, 51.61, 47.61, 46.78, 45.91, 41.70, 41.34, 39.33, 38.13, 37.81, 37.00, 33.92, 33.20, 33.01, 32.89, 32.64, 32.44, 30.78, 28.19, 27.98, 27.75, 25.99, 23.72, 23.63, 23.48, 23.12, 18.28, 16.90, 16.85, 15.44.

C4-MOP, a white solid, yield 60 %. ESI-MS (+): m/z 618.6; HRMS (ESI): m/z calcd. for $C_{40}H_{60}NO_4$: 618.4522, found 618.4519; ^{1}H NMR (400 MHz, DMSO-d_6, ppm): δ = 9.09 (d, 2 × 1H, *J* = 5.96 Hz, pyridine-H), 8.61 (t, 1H, *J* = 7.80 Hz, pyridine-H), 8.16 (t, 2 × 1H, *J* = 6.84 Hz, pyridine-H), 5.18 (t, 1H, 12-CH=C), 4.63 (t, 2H, *J* = 7.36 Hz, N-CH_2), 4.38 (m, 1H, 3-CH-O-), 3.53 (s, 3H, OCH_3), 2.45 (t, 2H, *J* = 8.72 Hz, O=C-CH_2), 2.21 (m, 2H, NCH_2CH_2), 1.10, 0.88, 0.80, 0.79, 0.65 (s, 7 × 3H, 7 × CH_3); ^{13}C NMR (100 MHz, $CDCl_3$, ppm): 178.33 (O=C-OCH_3), 172.21 (3-O-C=O), 145.62 (CH=C-), 145.31, 143.89, 128.65 (5C, pyridine-C), 122.24 (CH=C-), 81.94 (3-CH-O), 60.79, 55.33, 51.61, 47.59, 46.74, 45.90, 41.67, 41.31, 39.31, 38.11, 37.80, 36.96, 33.89, 33.17, 32.60, 32.41, 30.75, 30.63, 28.30, 27.72, 27.30, 25.98, 23.69, 23.45, 23.08, 18.24, 16.86, 15.42.

Acknowledgements

This work is supported by NSFC (Nos. 21172130, 21472108) and NBRP of China (973 Program, No. 2012CB821600); J.H. is grateful to the support of Scientific Research Foundation for the Returned Overseas Chinese Scholars, State Education Ministry; We thank Mr. W. Shi for the theoretical computation, and Dr. Dan Menasco for correcting the language.

Notes and references

1 A. Eschenmoser, L. Ruzicka, O. Jeger and D. Arigoni, *Helv. Chim. Acta*, 1955, **38**, 1890; A. Eschenmoser and D. Arigoni, *Helv. Chim. Acta*, 2005, **88**, 3011.
2 N. Miura, Y. Matsumoto, S. Miyairi, S. Nishiyama and A. Naganuma, *Mol. Pharmacol.*, 1999, **56**, 1324; V. Zuco, R. Supino, S. C. Righetti, L. Cleris, E. Marchesi, C. Gambacorti-Passerini and F. Formelli, *Cancer Lett.*, 2002, **175**, 17; H. Kuzuhara, S. Nishiyama, N. Minowa and K. Sasaki, *J. Nat. Med.*, 2006, **60**, 113; N. H. Buus, N. C. Hansson, R. Rodriguez-Rodriguez, E. Stankevicius, M. R. Andersen and U. Simonsen, *Eur. J. Pharmacol.*, 2011, **670**, 519; G. Sharma, S. Kar, S. Palit and P. K. Das, *J. Cell. Physiol.*, 2012, **227**, 1923.
3 B. G. Bag, G. C. Maity and S. R. Pramanik, *Supramol. Chem.*, 2005, **17**, 383; B. G. Bag and R. Majumdar, *RSC Adv.*, 2012, **2**, 8623; B. G. Bag and R. Majumdar, *RSC Adv.*, 2014, **4**, 53327; B. G. Bag, C. Garai, R. Majumdar and M. Laguerre, *Struct. Chem.*, 2012, **23**, 393.
4 B. G. Bag, S. K. Dinda, P. P. Dey, V. A. Mallia and R. G. Weiss, *Langmuir*, 2009, **25**, 8663; B. G. Bag and S. S. Dash, *Nanoscale*, 2011, **3**, 4564; B. G. Bag and K. Paul, *Asian J. Org. Chem.*, 2012, **1**, 150.
5 J. Hu, M. Zhang and Y. Ju, *Soft Matter*, 2009, **5**, 4971; J. R. Lu, J. Hu, Y. Song and Y. Ju, *Org. Lett.*, 2011, **13**, 3372; J. R. Lu, J. Hu, C. L. Liu, H. X. Gao and Y. Ju, *Soft Matter*, 2012, **8**, 9576; J. R. Lu, Y. X. Gao, J. D. Wu and Y. Ju, *RSC Adv.*, 2013, **3**, 23548; J. D. Wu, J. R. Lu, J. Hu, Y. X. Gao, Q. Ma and Y. Ju, *RSC Adv.*, 2013, **3**, 24906; J. R. Lu, J. D. Wu and Y. Ju, *New J. Chem.*, 2014, **38**, 6050.
6 A. Saha, J. Adamcik, S. Bolisetty, S. Handschin and R. Mezzenga, *Angew. Chem., Int. Ed.*, 2015, **54**, 5408.
7 Y. P. Wang, H. P. Xu and X. Zhang, *Adv. Mater.*, 2009, **21**, 2849; C. Wang, Z. Q. Wang and X. Zhang, *Acc. Chem. Res.*, 2012, **45**, 608; T. Shimizu, M. Masuda and H. Minamikawa, *Chem. Rev.*, 2005, **105**, 1401; T. G. Barclay, K. Constantopoulos and J. Matisons, *Chem. Rev.*, 2014, **114**, 10217; K. R. Raghupathi, J. Guo, O. Munkhbat, P. Rangadurai and S. Thayumanavan, *Acc. Chem. Res.*, 2014, **47**, 2200; S. Liu, P. C. Zhang, S. R. Banerjee, J. D. Xu, M. G. Pomper and H. G. Cui, *Nanoscale*, 2015, **7**, 9462; K. R. Raghupathi, U. Sridhar, K. Byrne, K. Raghupathi and S. Thayumanavan, *J. Am. Chem. Soc.*, 2015, **137**, 5308; B. Song, B. Liu, Y. Z. Jin, X. X. He, D. T. Tang, G. L. Wu and S. C. Yin, *Nanoscale*, 2015, **7**, 930; N. Goyal, S. Cheuk and G. J. Wang, *Tetrahedron*, 2010, **66**, 5962; G. J. Wang, H. Yang, S. Cheuk and S. Coleman, *Beilstein J. Org. Chem.*, 2011, **7**, 234.
8 M. J. Clemente, P. Romero, J. L. Serrano, J. Fitremann and L. Oriol, *Chem. Mater.*, 2012, **24**, 3847; K. R. Wang, H. W. An, L. Wu, J. C. Zhang and X. L. Li, *Chem. Commun.*, 2012, **48**, 5644; C. X. Liu, Q. X. Jin, K. Lv, L. Zhang and M. H. Liu, *Chem. Commun.*, 2014, **50**, 3702; R. Oda, I. Huc and S. J. Candau, *Angew. Chem., Int. Ed.*, 1998, **37**, 2689; M. R. Molla and S. Ghosh, *Chem. -Eur. J.*, 2012, **18**, 1290; A. Das and S. Ghosh, *Angew. Chem., Int. Ed.*, 2014, **53**, 1092; N. Suthiwangcharoen, T. Li, L. Wu, H. B. Reno, P. Thompson and Q. Wang, *Biomacromolecules*, 2014, **15**, 948.
9 Y. Kuang, J. F. Shi, J. Li, D. Yuan, K. A. Alberti, Q. B. Xu and B. Xu, *Angew. Chem., Int. Ed.*, 2014, **53**, 8104.
10 M. Ma, Y. Kuang, Y. Gao, Y. Zhang, P. Gao and B. Xu, *J. Am. Chem. Soc.*, 2010, **132**, 2719; S. Shin, S. Lim, Y. Kim, T. Kim, T. -L. Choi and M. Lee, *J. Am. Chem. Soc.*, 2013, **135**, 2156.
11 C. Wang, S. C. Yin, S. L. Chen, H. P. Xu, Z. Q. Wang and X. Zhang, *Angew. Chem., Int. Ed.*, 2008, **47**, 9049; K. Liu, C. Wang, Z. B. Li and X. Zhang, *Angew. Chem., Int. Ed.*, 2011, **50**, 4952; G. L. Wu, J. Thomas, M. Smet, Z. Q. Wang and X. Zhang, *Chem. Sci.*, 2014, **5**, 3267; X. J. Wu, S. J. Ji, Y. Li, B. Z. Li, X. L. Zhu, K. Hanabusa and Y. G. Yang, *J. Am. Chem. Soc.*, 2009, **131**, 5986.
12 E. Yashima, T. Matsushima and Y. Okamoto, *J. Am. Chem. Soc.*, 1997, **119**, 6345; A. Ajayaghosh, C. Vijayakumar, R. Varghese and S. J. George, *Angew. Chem., Int. Ed.*, 2006, **45**, 456; Y. Ogawa, C. Yoshiyama and T. Kitaoka, *Langmuir*, 2012, **28**, 4404.
13 R. L. B. Selinger, J. V. Selinger, A. P. Malanoski and J. M. Schnur, *Phys. Rev. Lett.*, 2004, **93**, 158103; J. X. Cui, A. H. Liu, Y. Guan, J. Zheng, Z. H. Shen and X. H. Wan, *Langmuir*, 2010,

26, 3615; P. F. Duan, H. Cao, L. Zhang and M. H. Liu, *Soft Matter*, 2014, **10**, 5428; L. Zhang, L. Qin, X. F. Wang, H. Cao and M. H. Liu, *Adv. Mater.*, 2014, **26**, 6959; X. F. Wang, P. F. Duan and M. H. Liu, *Chem. Commun.*, 2012, **48**, 7501; J. Kumar, T. Nakashima and T. Kawai, *Langmuir*, 2014, **30**, 6030; J. J. Li, K. Q. Fan, X. D. Guan, Y. Z. Yu and J. Song, *Langmuir*, 2014, **30**, 13422; A. Gopal, M. Hifsudheen, S. Furumi, M. Takeuchi and A. Ajayaghosh, *Angew. Chem., Int. Ed.*, 2012, **51**, 10505.

14 Z. Y. Xu, J. X. Peng, N. Yan, H. Yu, S. S. Zhang, K. Q. Liu and Y. Fang, *Soft Matter*, 2013, **9**, 1091.

15 F. Würthner, T. E. Kaiser and C. R. Saha-Möller, *Angew. Chem., Int. Ed.*, 2011, **50**, 3376; H. Kar, D. W. Gehrig, F. Laquai and S. Ghosh, *Nanoscale*, 2015, **7**, 6729; M. Dubey, A. Kumar and D. S. Pandey, *Chem. Commun.*, 2014, **50**, 1675; S. K. Samanta and S. Bhattacharya, *Chem. Commun.*, 2013, **49**, 1425; J. Kärnbratt, M. Gilbert, J. K. Sprafke, H. L. Anderson and B. Albinsson, *J. Phys. Chem. C*, 2012, **116**, 19630; Y. X. Gao, J. R. Lu, J. D. Wu, J. Hu and Y. Ju, *RSC Adv.*, 2014, **4**, 63539.

16 M. Bhat and V. G. Gaikar, *Langmuir*, 2000, **16**, 1580; M. J. Hostetler, J. J. Stokes and R. W. Murray, *Langmuir*, 1996, **12**, 3604; N. Yamada, K. Ariga, M. Naito, K. Matsubara and E. Koyama, *J. Am. Chem. Soc.*, 1998, **120**, 12192.

17 G. C. Yu, X. Z. Yan, C. Y. Han and F. H. Huang, *Chem. Soc. Rev.*, 2013, **42**, 6697.

18 U. Lewandowska, W. Zajaczkowski, L. Chen, F. Bouillière, D. Wang, K. Koynow, W. Pisula, K. Müllen and H. Wennemers, *Angew. Chem., Int. Ed.*, 2014, **53**, 12537; C. Janiak, *J. Chem. Soc., Dalton Trans.*, 2000, 3885.

19 L. Zhang, X. F. Wang, T. Y. Wang and M. H. Liu, *Small*, 2015, **11**, 1025; Z. C. Shen, T. Y. Wang and M. H. Liu, *Angew. Chem., Int. Ed.*, 2014, **53**, 13424; A. Sánchez-Ferrer, J. Adamcik and R. Mezzenga, *Soft Matter*, 2012, **8**, 149.

20 D. K. Smith, *Chem. Soc. Rev.*, 2009, **38**, 684.

21 J. Hu, L. B. Yu, M. Zhang and Y. Ju, *Chin. J. Chem.*, 2011, **29**, 1139.